Dynamic Recrystallization during Hot Deformation of Aluminum: A Study Using Processing Maps

N. RAVICHANDRAN and Y.V.R.K. PRASAD

The hot deformation behavior of aluminum of different purities has been studied in the temperature range of 250 °C to 600 °C and strain-rate range of 10^{-3} to 10^{2} s^{-1}. On the basis of the flow stress data, the strain-rate sensitivity (m) of the material is evaluated and used for establishing power dissipation maps following the Dynamic Materials Model. These maps depict the variation of the efficiency of power dissipation [$\eta = 2m/(m + 1)$] with temperature and strain rate. A domain of dynamic recrystallization (DRX) could be identified in these maps. While the strain rate at which the efficiency peak occurred in this domain is 10^{-3} s^{-1}, the DRX temperature is purity dependent and is 375 °C for 99.999 pct Al, 450 °C for 99.995 pct Al, 550 °C for 99.94 pct Al, and 600 °C for 99.5 pct Al. The maximum efficiency of power dissipation for DRX in aluminum is about 55 pct. The sigmoidal increase of grain size with temperature in the DRX domain and the decrease in the DRX temperature with increase in the purity of aluminum are very similar to that observed in static recrystallization, although DRX occurred at much higher temperatures.

I. INTRODUCTION

THE mechanism of hot deformation in aluminum and its alloys has been studied extensively[1–7] using laboratory tests such as tension, compression, and torsion, as well as metalworking processes like rolling and extrusion. In pure aluminum, it is considered that the mechanism of softening is essentially dynamic recovery, which occurs readily due to the high stacking fault energy (SFE) of aluminum. In view of this, it is generally stated that aluminum does not dynamically recrystallize, as there is no direct microstructural evidence after hot deformation. However, dynamic recrystallization (DRX) is reported in aluminum deformed at large strains and elevated temperatures.[8–11] McQueen and co-workers[12,13] called this "geometric" DRX, the process which increases the large-angle grain boundary area without changing the total number of grains in the specimen. Recent studies of the influence of strain-rate changes at 450 °C on the stress-strain behavior and microstructural development in commercial aluminum showed that the transient behavior is strain rate-dependent, and the strain required to obtain equilibrium subgrain structure is higher for lower strain rates.[14,15] In aluminum alloys, the occurrence of DRX is attributed to the lowering of SFE caused by solute additions, particularly magnesium.[5,6,7] The presence of fine particles may also cause DRX in aluminum.[4] The aim of the present investigation is to examine whether DRX occurs in aluminum and, if so, study its characteristics.

Earlier investigations[4,6,16,17] have followed a kinetic approach for analyzing the deformation behavior using an Arrhenius-type rate equation. However, the stress exponent was found to be temperature- and strain rate-dependent, and so the interpretation of the apparent activation parameter is complex. In view of this, a different approach based on processing maps has been followed. In the processing map developed by Raj,[18] on the basis of atomistic mechanisms, a regime of dynamic recrystallization is depicted at high temperatures. A newer approach is that using the Dynamic Materials Model,[19] which helps in mapping the characteristics of power dissipation by microstructural changes as a function of temperature and strain rate using the strain-rate sensitivity parameter. The power dissipation map helps in delineating the domains within which particular microstructural mechanisms dominate. As any recrystallization process is sensitive to the purity of the material, processing maps on aluminum of different purities have been established in this study.

N. RAVICHANDRAN, Graduate Student, and Y.V.R.K. PRASAD, Professor, are in the Department of Metallurgy, Indian Institute of Science, Bangalore 560 012, India.

Manuscript submitted October 30, 1990.

II. EXPERIMENTAL

Aluminum of four different purities, namely, 99.999, 99.995, 99.94, and 99.5 pct Al, were used in this investigation, and these will be referred to as 5-9, 4-9, 3-9, and 2-9 purity aluminum, respectively. Extruded rods of 12-mm diameter were the starting materials for machining specimens for hot compression testing. Cylindrical specimens of 10-mm diameter and 15-mm height were machined such that their faces were parallel. Concentric grooves of about 0.5-mm depth were engraved on the specimen faces to facilitate the retention of the lubricant. A 1-mm 45-deg chamfer was given to the edges of the face to avoid foldover in the initial stages of the compression. A 0.5-mm-diameter hole was drilled to a depth of 5 mm at half the height of each specimen for the insertion of a thermocouple. The specimens were all annealed at 550 °C for 0.5 hours, and the resulting average grain diameters were 0.32, 0.76, 0.063, and 0.083 mm, respectively, for the four different purities mentioned above.

Hot compression tests were conducted in the temperature range of 250 °C to 600 °C and in the strain-rate range of 10^{-3} to 10^{2} s^{-1}. A computer-controlled servo-hydraulic machine (DARTEC, United Kingdom) was used in this investigation. The machine had the facility for an

exponential decay of actuator speed to give constant true strain rates during the tests. In arriving at the exponential decay equation for the stroke-time variation, the small elastic deflections of the machine and the grips were neglected. The temperature control was within ±2 °C, and the adiabatic temperature rise during compression was measured with a thermocouple embedded in the specimen. The static recrystallization temperatures for aluminum of the four different purities were determined by cold upsetting the material to a 50 pct strain and annealing for 1 hour at different temperatures in the range of 100 °C to 500 °C. Hardness measurements were used to evaluate the static recrystallization temperature. The deformed specimens were sectioned vertically, and microstructural examination and grain size measurements were conducted using standard metallographic techniques. Microstructures of air-cooled as well as water-quenched specimens deformed at selected regions of the power dissipation maps were examined. A scanning electron microscope was used for documenting the microstructures. The specimens were electropolished in a solution of 12.5 pct perchloric acid, 20 pct glycerol, and 67.5 pct methanol. In the case of water quenching, the cooling rate was about 3×10^3 °C/s, and the delay times were less than 3 seconds.

III. RESULTS

The load-stroke curves obtained in hot compression are converted into true stress-true plastic strain curves by subtracting the elastic portion of strain and using standard equations for true stress and true strain calculations. Typical stress-strain curves recorded at 300 °C and 400 °C at different strain rates for 5-9 aluminum are shown in Figures 1(a) and (b), respectively. The curves corresponding to strain rates of 0.001 and 0.01 s^{-1} showed steady-state behavior beyond a strain of about 0.1, while at higher strain rates, strain hardening is observed at 300 °C. The strain rate at which this changeover from steady-state to strain-hardening behavior occurred is higher at higher temperatures. At 400 °C, the material showed strain hardening at all strain rates. The behavior of aluminum of other purities is similar to that described above.

The variation of flow stress (σ) with temperature (T), strain rate ($\dot{\varepsilon}$), and strain (ε) for aluminum of different purities is shown in Tables I through IV. The flow stress is corrected for the adiabatic temperature rise using linear interpolation of log σ *vs* $(1/T)$ data, and this correction was found to be significant at lower temperatures and higher strain rates.

Power dissipation maps were constructed using the data described above and the principles of the Dynamic Materials Model.[19] The map software adopts the following procedure: log flow stress *vs* log strain-rate data at a constant temperature and strain are fitted using a cubic spline, and the strain-rate sensitivity (m) is calculated as a function of strain rate. This is repeated at different temperatures. The efficiency of power dissipation through microstructural changes [$\eta = 2m/(m + 1)$] is then calculated from a set of m values as a function of strain rate and temperature and plotted as a three-dimensional (3-D) map. The 3-D variation is better viewed as an iso-efficiency contour map in the strain rate-temperature plane.

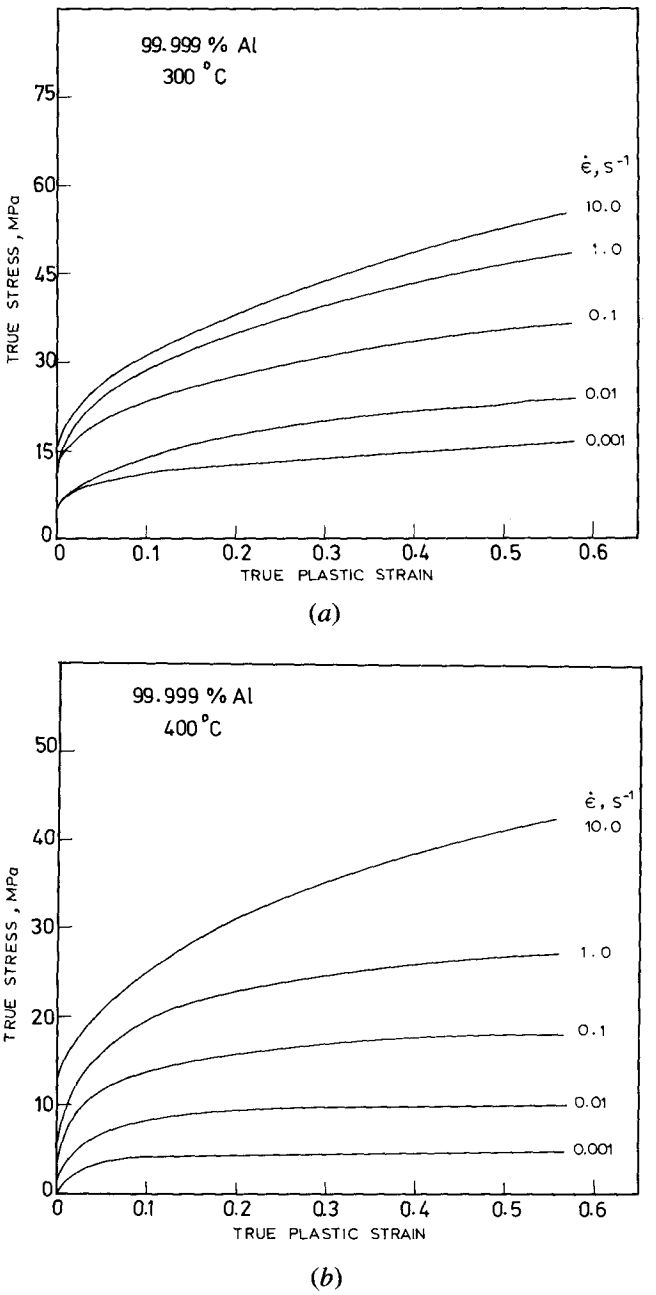

Fig. 1 — True stress-true plastic strain curves for 99.999 pct Al obtained in compression at (*a*) 300 °C and (*b*) 400 °C at different strain rates.

The power dissipation map for 5-9 aluminum at a strain of 0.3 is shown in Figure 2(a) in 3-D and in Figure 2(b) as a contour map. Note that η is plotted in percent in the figures of this article *vs* the definition stated above. A strain of 0.3 is selected, since this value is large enough to effect homogeneous deformation and small enough to minimize the influence of barreling. However, the maps obtained at strains of 0.2 and 0.4 (Figures 3 and 4) are similar. The maps obtained with aluminum of other purities are also found to be essentially independent of strain.

Table I. Flow Stress Values (in MPa) of 5-9 Pure Aluminum at Different Strain Rates and Temperatures for Various Strains (Corrected for Adiabatic Temperature Rise)

Strain	Strain Rate (s^{-1})	Temperature (°C)				
		300	350	400	450	500
0.1	0.001	10.8	8.1	4.3	2.9	1.7
	0.01	13.0	12.4	8.4	5.1	4.0
	0.1	23.1	20.3	13.9	10.5	7.8
	1.0	23.4	19.6	14.3	11.1	9.5
	10.0	26.4	25.2	19.9	17.6	14.7
0.2	0.001	12.4	8.1	4.3	3.1	1.8
	0.01	17.7	14.1	9.5	5.5	4.1
	0.1	27.8	24.0	15.8	11.3	8.5
	1.0	27.9	23.2	16.9	12.5	10.5
	10.0	33.4	31.3	24.3	21.1	17.4
0.3	0.001	13.5	8.1	4.6	3.4	2.0
	0.01	20.1	14.9	9.6	5.7	4.1
	0.1	30.8	26.2	16.5	12.1	8.8
	1.0	30.9	25.4	18.0	13.0	10.9
	10.0	38.7	35.8	27.5	23.1	19.0
0.4	0.001	14.6	8.2	4.8	3.6	2.0
	0.01	21.7	15.6	9.9	6.2	4.2
	0.1	33.0	28.0	17.4	12.6	8.9
	1.0	32.9	26.6	18.6	13.2	11.1
	10.0	42.9	39.3	29.6	24.5	20.0
0.5	0.001	15.5	8.5	4.9	3.8	2.0
	0.01	22.9	16.4	9.9	6.3	4.4
	0.1	35.3	30.5	18.1	13.2	9.0
	1.0	34.1	27.3	19.0	13.7	11.5
	10.0	46.4	41.7	30.7	25.3	20.6

Table II. Flow Stress Values (in MPa) of 4-9 Pure Aluminum at Different Strain Rates and Temperatures for Various Strains (Corrected for Adiabatic Temperature Rise)

Strain	Strain Rate (s^{-1})	Temperature (°C)					
		250	300	350	400	450	500
0.1	0.001	13.4	9.9	5.6	3.4	2.1	1.6
	0.01	22.6	13.0	11.5	8.6	5.9	3.9
	0.1	26.5	22.6	16.3	13.0	10.3	7.5
	1.0	35.7	21.8	21.9	19.5	15.3	11.6
	10.0	42.4	28.7	27.5	23.1	18.7	13.6
	100.0	47.3	40.3	31.8	25.7	22.3	18.6
0.2	0.001	17.9	11.7	6.7	4.1	2.3	1.7
	0.01	30.7	17.7	13.1	9.5	6.4	4.0
	0.1	35.7	29.2	20.0	15.2	11.1	8.0
	1.0	47.5	29.4	28.4	24.2	17.9	13.0
	10.0	56.0	40.0	35.9	29.7	23.4	17.2
	100.0	59.9	54.5	40.7	31.0	28.2	22.0
0.3	0.001	20.4	12.5	7.2	4.1	2.4	1.6
	0.01	36.3	20.1	14.1	9.9	6.5	4.1
	0.1	42.7	33.6	21.7	16.0	11.6	8.1
	1.0	58.0	34.8	32.8	26.8	19.0	13.7
	10.0	69.4	47.9	42.3	34.2	26.7	19.0
	100.0	74.4	68.9	50.6	36.1	32.0	24.5
0.4	0.001	21.9	13.1	7.5	4.3	2.6	1.6
	0.01	43.0	21.7	15.4	10.5	6.8	4.3
	0.1	48.2	36.8	22.8	16.5	12.2	8.3
	1.0	69.7	38.6	36.2	28.9	19.9	14.2
	10.0	81.2	54.1	47.3	37.2	28.6	19.9
	100.0	87.3	77.9	51.1	39.1	34.2	26.5

Table III. Flow Stress Values (in MPa) of 3-9 Pure Aluminum at Different Strain Rates and Temperatures for Various Strains (Corrected for Adiabatic Temperature Rise)

Strain	Strain Rate (s^{-1})	Temperature (°C)					
		300	350	400	450	500	550
0.1	0.001	19.1	13.0	7.9	5.8	3.4	2.0
	0.01	27.1	18.2	12.9	9.1	5.7	3.7
	0.1	36.0	24.8	19.3	15.0	9.7	7.0
	1.0	40.8	35.8	26.2	20.2	15.1	12.0
	10.0	48.1	39.6	34.7	27.5	20.7	17.4
	100.0	50.0	38.8	49.2	34.1	27.4	20.9
0.2	0.001	21.0	13.7	8.6	5.9	3.4	2.0
	0.01	32.9	20.2	14.1	9.5	5.9	3.8
	0.1	43.0	28.7	21.1	16.1	10.1	7.3
	1.0	49.0	42.4	30.0	22.2	16.4	12.7
	10.0	57.4	46.7	40.0	31.7	23.4	19.5
	100.0	61.9	47.2	54.1	39.9	33.6	24.9
0.3	0.001	21.8	14.4	8.9	5.9	3.4	1.9
	0.01	37.2	21.7	14.8	9.8	5.9	3.9
	0.1	49.1	31.5	22.2	16.5	10.2	7.5
	1.0	56.9	48.5	32.5	23.3	16.8	12.9
	10.0	66.5	52.9	45.0	34.8	24.7	20.4
	100.0	69.8	52.8	58.0	44.0	37.1	26.9
0.4	0.001	22.8	15.0	9.6	6.1	3.6	1.9
	0.01	41.0	23.1	15.4	10.0	6.0	4.1
	0.1	55.0	33.5	23.2	17.0	10.7	7.7
	1.0	64.9	53.7	34.3	24.0	17.0	13.1
	10.0	75.2	59.0	50.0	36.7	25.8	21.5
	100.0	77.7	56.9	61.1	45.8	38.2	27.5
0.5	0.001	24.3	15.3	10.2	6.2	3.6	1.9
	0.01	46.0	24.2	15.8	10.2	6.1	4.2
	0.1	61.0	36.0	24.2	17.4	10.9	7.8
	1.0	70.5	59.7	36.7	24.7	17.1	13.3
	10.0	84.0	64.7	54.9	38.5	26.3	21.7
	100.0	80.3	61.6	65.2	47.4	39.2	28.9

Maps corresponding to a strain of 0.3 are shown for the aluminum of the other three purities shown in Figures 5 through 7. Referring to Figure 7, the map for 2-9 purity aluminum has only one domain with the power dissipation efficiency peak of 55 pct at 600 °C and a strain rate of about 10^{-3} s^{-1}. With increasing purity, this peak efficiency domain has rotated slightly clockwise toward lower strain rates and lower temperatures. In 3-9 purity aluminum, the domain is centered at 500 °C and 10^{-3} s^{-1} (Figure 6); in 4-9 purity, the domain is at 475 °C and 10^{-3} s^{-1} (Figure 5); and in 5-9 purity, the domain is at about 360 °C and 10^{-3} s^{-1} (Figure 2(b)). In 5-9 purity, a new domain has also appeared at 500 °C and 10^{-3} s^{-1} strain rate (Figure 2(b)).

IV. DISCUSSION

A. *Interpretation of Power Dissipation Maps*

The basis for the power dissipation maps is the Dynamic Materials Model developed by Prasad *et al.*[19] and reviewed recently by Gegel *et al.*[20] This model is a continuum one and follows a systems approach. The workpiece is considered as a dissipator part of processing the system, and its constitutive equation describes the manner in which the energy is converted at any instant into a form, usually thermal and microstructural, which is nonrecoverable by the system. The dissipator element can be considered to be nonlinear, dynamic, and irreversible. At any instant, the total power dissipated is considered to consist of two complementary parts, G—content representing the temperature rise—and J—co-content representing the dissipation through metallurgical processes. The factor that partitions power between G and J is the strain-rate sensitivity (m) of flow stress. The J co-content is given by[19,20]

$$J = \sigma\dot{\varepsilon}m/(m + 1) \qquad [1]$$

where σ = flow stress and $\dot{\varepsilon}$ = strain rate. For an ideal linear dissipator, $m = 1$ and $J = J_{max} = \sigma\dot{\varepsilon}/2$. The efficiency of power dissipation for a nonlinear dissipator may be expressed as a dimensionless parameter:

$$\eta = J/J_{max} = 2m/(m + 1) \qquad [2]$$

The variation of η with temperature and strain rate represents the power dissipation characteristics of the workpiece material.

As the system is irreversible, the dissipated power is related to the rate of entropy production, which is always positive.[21] In systems which have a high rate of entropy production, the concepts of self-organization of chaotic systems proposed by Prigogine[22] are applicable, and the power dissipation maps may be interpreted to represent

Table IV. Flow Stress Values (in MPa) of 2-9 Pure Aluminum at Different Strain Rates and Temperatures for Various Strains (Corrected for Adiabatic Temperature Rise)

Strain	Strain Rate (s^{-1})	Temperature (°C)								
		200	250	300	350	400	450	500	550	600
0.1	0.001	174	136	69.2	37.4	22.4	10.7	6.8	3.6	2.6
	0.01	192	127	88.0	48.3	25.2	16.3	10.2	6.7	5.8
	0.1	207	144	100	56.7	38.3	26.4	17.5	12.9	11.9
	1.0	274	185	109	68.8	47.2	33.9	28.9	20.1	15.4
	10.0	286	197	122	87.8	63.6	47.8	38.6	32.1	22.0
	100.0	295	206	139	96.4	71.8	55.1	49.7	38.0	26.4
0.2	0.001	173	131	66.7	36.6	22.2	10.8	6.8	3.7	2.8
	0.01	190	126	87.3	47.4	26.3	17.6	10.7	6.9	5.6
	0.1	205	143	99.7	58.1	38.9	27.0	18.0	13.0	12.1
	1.0	275	185	111	69.9	49.1	35.8	30.2	21.0	15.8
	10.0	290	198	123	91.0	66.6	50.1	41.1	32.5	23.6
	100.0	295	211	141	101	76.1	58.6	53.7	41.9	28.7
0.3	0.001	172	127	65.9	36.3	22.0	10.9	7.1	3.8	2.8
	0.01	190	125	86.9	47.4	27.0	18.2	11.6	6.9	5.9
	0.1	204	143	100	58.7	39.8	27.8	18.8	13.3	12.5
	1.0	274	186	112	70.3	50.8	36.7	30.9	21.9	16.2
	10.0	284	199	123	92.6	68.8	52.4	43.0	33.4	24.9
	100.0	294	217	148	103	79.6	60.7	54.5	43.7	29.4
0.4	0.001	171	122	64.6	35.8	21.8	11.1	7.5	4.2	2.7
	0.01	188	123	86.1	47.5	27.7	18.7	11.8	7.0	6.1
	0.1	205	143	100	58.9	40.9	27.9	19.0	13.7	12.7
	1.0	274	187	112	72.4	51.6	37.2	31.5	22.2	16.5
	10.0	288	199	125	94.1	69.5	53.8	43.7	33.9	25.9
	100.0	294	222	151	107	81.9	61.9	55.3	43.8	29.0
0.5	0.001	170	121	64.0	35.8	21.5	11.2	7.7	4.3	2.6
	0.01	189	123	85.5	47.3	28.5	18.9	11.9	7.2	6.3
	0.1	206	143	100	59.8	41.4	28.0	19.5	14.1	13.2
	1.0	271	189	113	72.3	52.5	37.9	31.9	22.6	16.6
	10.0	289	200	126	95.6	72.0	55.0	44.3	34.8	26.0
	100.0	293	220	152	109	83.9	62.8	54.7	43.3	28.2

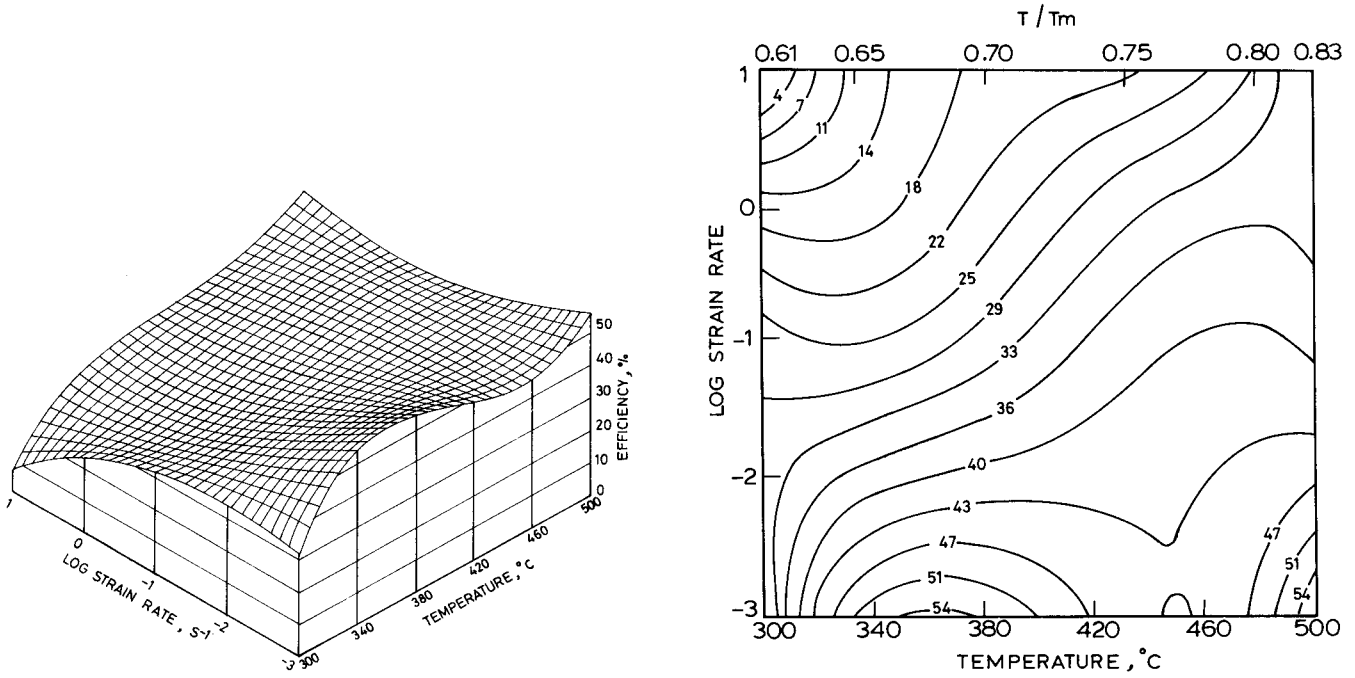

Fig. 2—(*a*) 3-D view of the variation of power dissipation efficiency with temperature and strain rate for 5-9 purity aluminum at a strain of 0.3. (*b*) Contour map with iso-efficiency contours of the efficiency of power dissipation for 5-9 purity aluminum corresponding to the 3-D map.

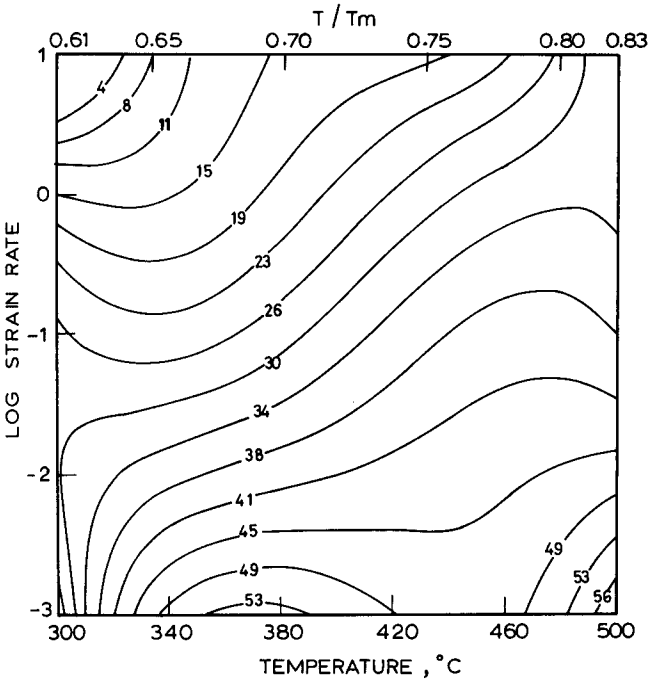

Fig. 3—Power dissipation map for 99.999 pct Al at a strain of 0.2 showing iso-efficiency contours. Numbers represent efficiency in percent.

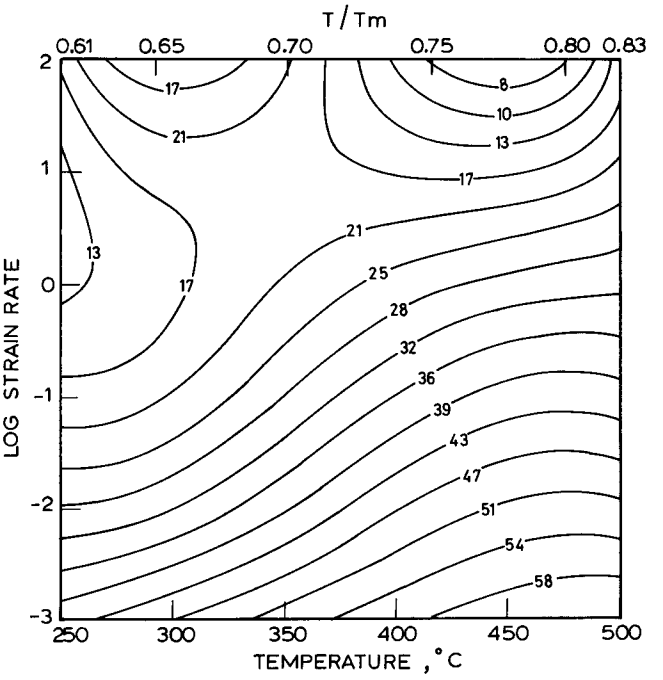

Fig. 5—Power dissipation map for 99.995 pct Al at a strain of 0.3 showing iso-efficiency contours. Numbers represent efficiency in percent.

the rate of excess entropy production. The maps then represent domains of local order (concentric iso-efficiency contours) corresponding to specific dissipative mechanisms (microstructures) separated by bifurcations which are probability-related. The domains are deterministic, kinetic laws are obeyed within the domain, and the dissipative structures characterize the domain.

The power dissipation maps are continuum maps; however, the domains can be interpreted in terms of specific atomistic processes. This can be done with the help of Raj maps.[18] In hot deformation, there are "safe" and "damage" mechanisms that occur at different strain-rate and temperature combinations. The safe mechanisms are dynamic recovery (lower temperature and strain rates) and DRX (higher temperature and intermediate strain rates). Microstructural damage due to wedge cracking

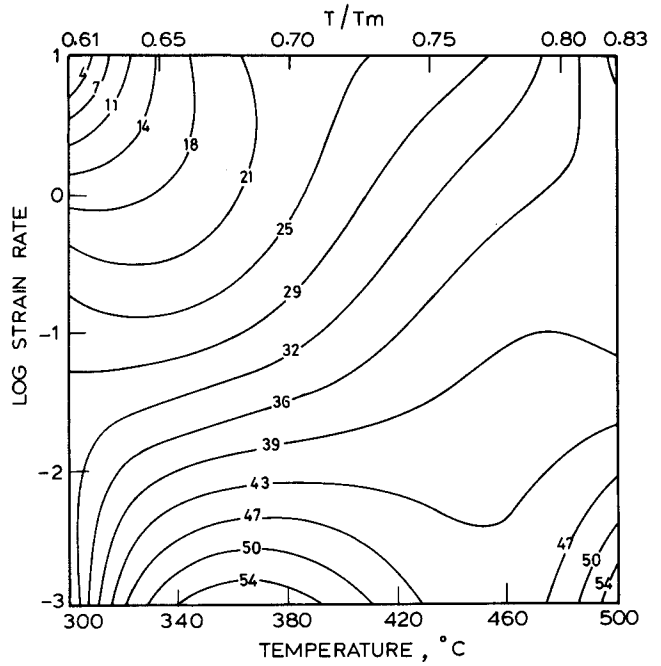

Fig. 4—Power dissipation map for 99.999 pct Al at a strain of 0.4 showing iso-efficiency contours. Numbers represent efficiency in percent.

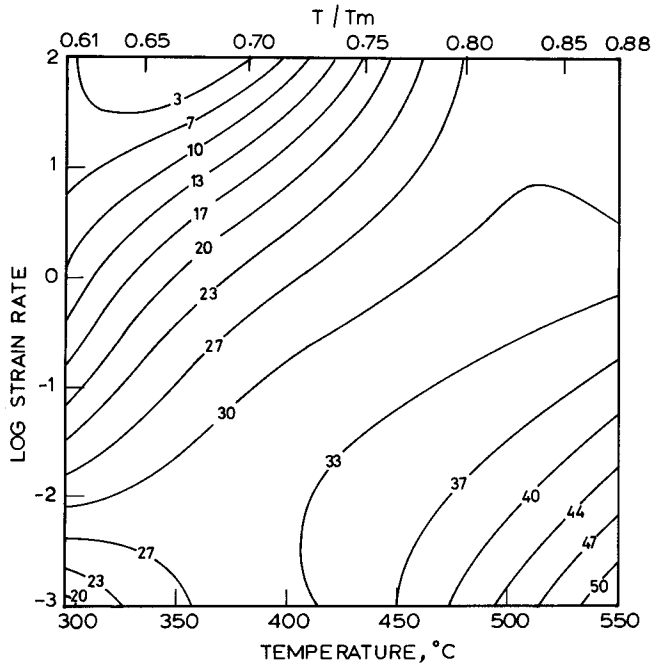

Fig. 6—Power dissipation map for 99.94 pct Al at a strain of 0.3 showing iso-efficiency contours. Numbers represent efficiency in percent.

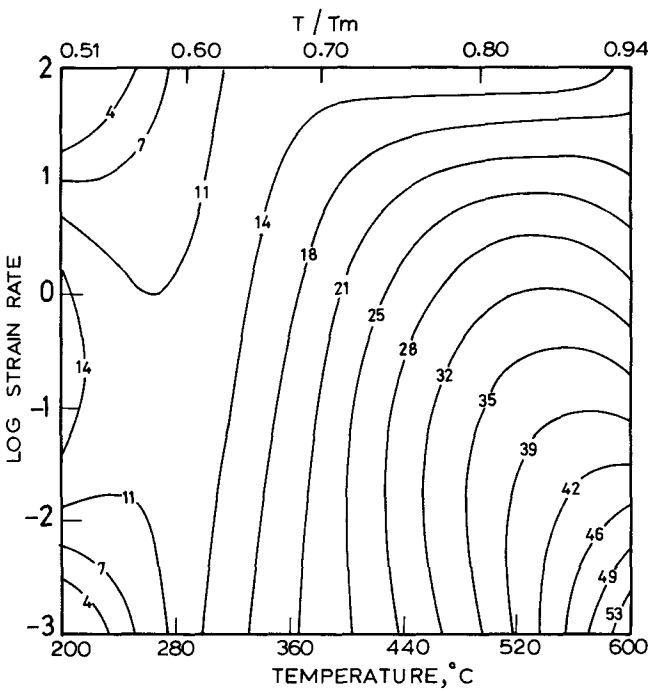

Fig. 7—Power dissipation map for 99.5 pct Al at a strain of 0.3 showing iso-efficiency contours. Numbers represent efficiency in percent.

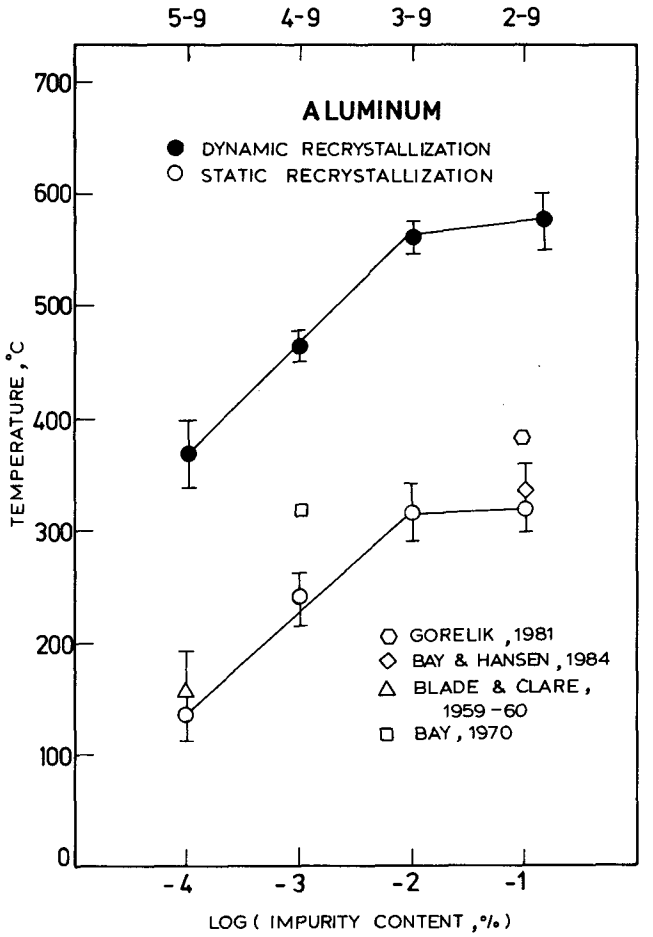

Fig. 8—Variation of recrystallization temperatures with purity in aluminum.

will occur at lower strain rates and higher temperatures; void formation at hard particles is dominant at high strain rates and low temperatures. The damage processes are very efficient in dissipating power through the generation of new surfaces, while the "safe" processes are less efficient, since power dissipation occurs by annihilation of dislocations or their groups. Out of the two safe processes, DRX has a higher efficiency than dynamic recovery. The DRX process has been shown[18] to occur in aluminum at 0.7 to $0.8T_m$ and at strain rates of about 0.1 s^{-1}.

B. *Characteristics of Dynamic Recrystallization*

On the basis of the above interpretation, the domain observed in the power dissipation maps (Figures 2 through 7) of aluminum represents the process of DRX and has a maximum efficiency of 50 to 55 pct. This interpretation is further confirmed by the observations described below concerning the effect of purity, the variation of grain size in the domain, and the ductility of the material.

1. *Effect of purity*

Taking the DRX temperature to be that at which the efficiency peak has occurred, the effect of purity on the DRX temperature is shown in Figure 8. The DRX temperature is higher at higher impurity contents, the effect being more significant at lower impurity content. The data for the effect of impurities on static recrystallization temperature are also shown in Figure 8 for comparison. The results of Blade *et al.*[23] on zone refined aluminum, Bay[24] on 99.9 pct aluminum, and Bay and Hansen[25] and Gorelik[26] on commercial aluminum are also included in Figure 8. The scatter in the data of these workers could be attributed to a large number of variables, such as the extent of cold work and the initial grain size that influence the static recrystallization process, as well as the differences in the chemical analysis employed in the various studies.

The effect of purity on static and DRX temperatures is strikingly similar, although the DRX temperature is much higher. This suggests that the domain represents the process of DRX and that the fundamental processes involved in the static and DRX are essentially the same.

2. *Grain size variations*

A typical microstructure in the DRX domain for the 5-9 aluminum is shown in Figure 9, which corresponds to the peak efficiency conditions (350 °C, 10^{-3} s^{-1}). The variations of the average grain diameter with temperature at the strain rate corresponding to the peak in the DRX domain (10^{-3} s^{-1}) is shown in Figure 10. While most of these data are for air-cooled specimens, the measurements on the quenched samples are shown for 5-9 aluminum for the purpose of comparison. In the DRX domain, the grain sizes measured on the quenched specimens are marginally smaller, and the variation of the grain size with temperature is essentially similar in the air-cooled and the quenched specimens. The grain size increases with temperature following a sigmoidal variation similar to that observed in static recrystallization. The temperature at which 50 pct change in grain size has occurred is matched with the temperature for the peak

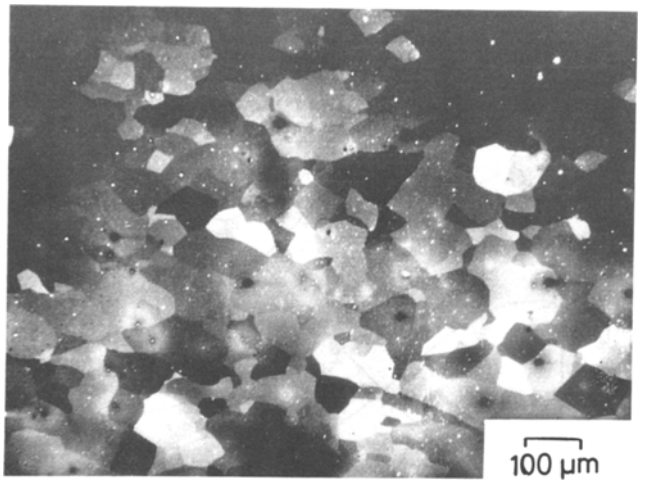

Fig. 9—Dynamically recrystallized microstructure of 5-9 aluminum deformed at 400 °C and strain rate of 0.001 s^{-1}.

efficiency. Similar to that followed for static recrystallization, this temperature may be termed as the DRX temperature. The similarity of grain size variations in static and DRX is seen using the data of Williams and Eborall,[27] data on static recrystallization of 4-9 purity aluminum, and the present data on 2-9 purity aluminum.

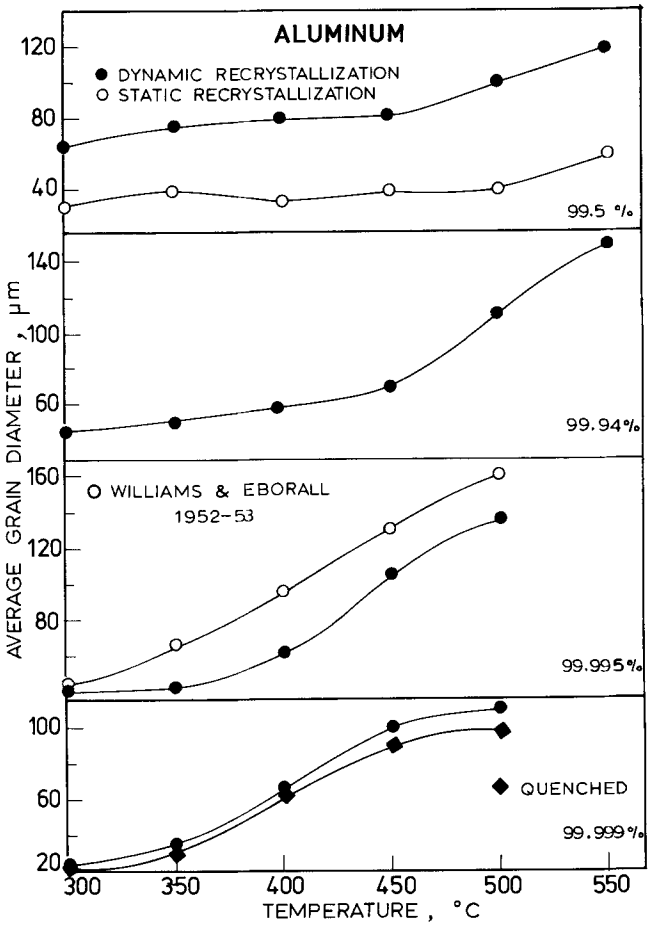

Fig. 10—Variation of grain size with temperature in DRX and static recrystallization of aluminum.

Microstructures away from the DRX domain, *e.g.*, at a strain rate of 1 s^{-1}, showed features different from those described above for the 5-9 purity aluminum. The microstructure of the sample deformed at 450 °C and 1 s^{-1} is given in Figure 11. The microstructure revealed inhomogeneous deformation which manifested itself in the form of localized shear bands indicating the onset of flow instability. However, the microstructure of the specimen deformed at 500 °C and 1 s^{-1} revealed the presence of intercrystalline cracks (Figure 12). It is possible that these cracks initiated at grain boundary triple junctions consequent to grain boundary sliding. Thus, the high-temperature domain (>450 °C) corresponds to the process of wedge cracking, as predicted also by Raj maps.[18] Owing to the presence of these microstructural inhomogeneities away from the DRX domain, the grain size variations do not represent the relevant dissipative processes.

3. *Ductility*

The variation of ductility in torsion with temperature of 99.999 pct Al was measured by Kassner *et al.*[28] at

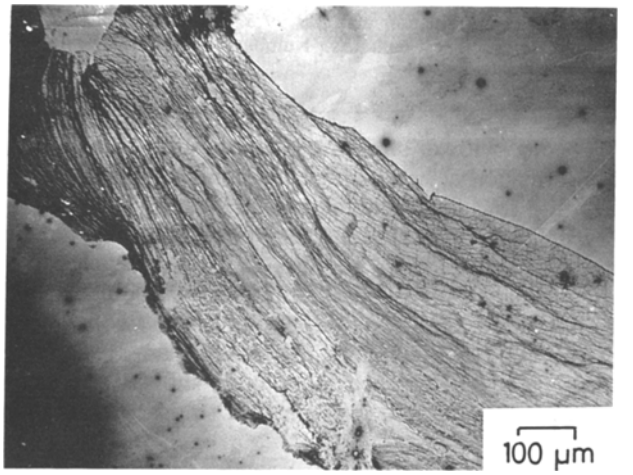

Fig. 11—Microstructure of 5-9 aluminum deformed at 450 °C and 1 s^{-1} showing localized shear bands.

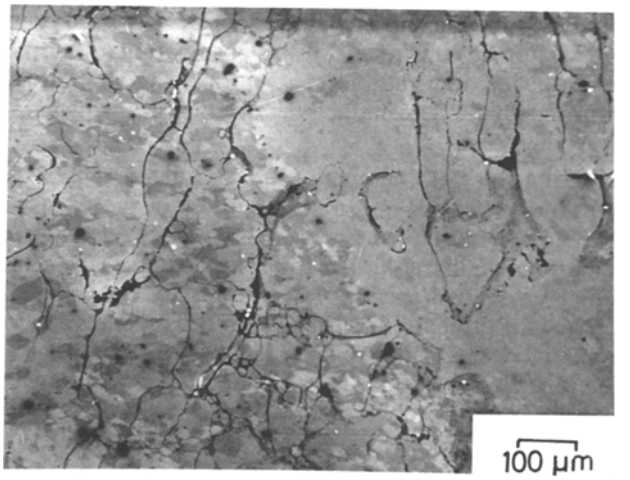

Fig. 12—Microstructure of 5-9 aluminum deformed at 500 °C and 1 s^{-1} revealing intercrystalline cracks.

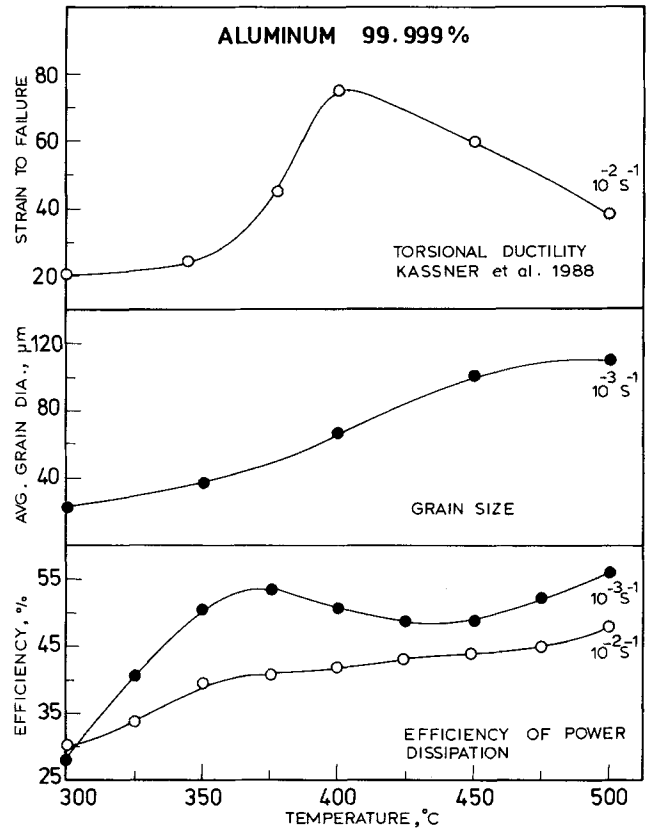

Fig. 13—Variation of the efficiency of power dissipation, average grain diameter with temperature in the DRX of 99.999 pct Al. The torsional ductility variation shown by Kassner *et al.*[28] is also shown.

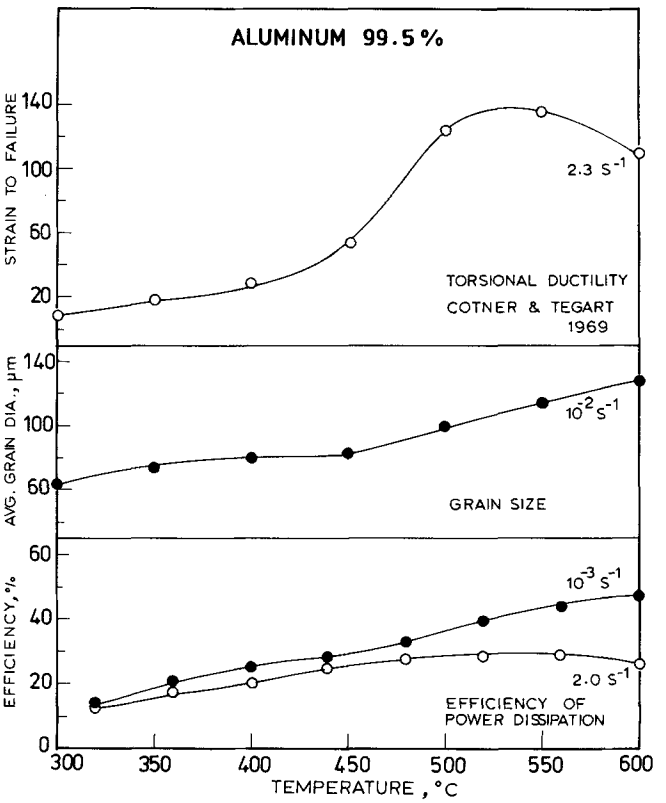

Fig. 14—Variation of the efficiency of power dissipation, average grain diameter with temperature in the DRX of 99.5 pct Al. The torsional ductility variation shown by Cotner and Tegart[29] is also shown.

a strain rate of 10^{-2} s^{-1}. This behavior is shown in Figure 13 and compared with the efficiency and grain size variation within the DRX domain. The temperature for the ductility peak which occurred at 400 °C coincided with that for the 50 pct change in grain size and the efficiency peak for the 10^{-2} s^{-1} strain rate. However, the temperature for the efficiency peak at 10^{-3} s^{-1} strain rate was lower by about 25 °C. At temperatures higher than 450 °C, the efficiency increased, and this corresponded to a separate high-temperature domain in the map. As there is no significant change in grain size, this domain can be interpreted in terms of the grain boundary sliding process, which may cause wedge cracks at grain boundary triple junctions. Wedge cracking reduces the ductility of the material, as seen in the results of Kassner *et al.*[28] The ductility results on the commercial purity Al (2-9) obtained by Cotner and Tegart[29] are shown in Figure 14; these also confirm the correlation between the ductility and efficiency of power dissipation in the DRX domain.

The above discussion indicates that the indicated domain observed in the maps represents the DRX process. In addition, there is a strong similarity between the characteristics of DRX and static recrystallization, although the former occurs at much higher temperatures. The efficiency of power dissipation reaches a maximum value of about 55 pct for the DRX process.

V. CONCLUSIONS

An analysis of the hot deformation behavior of aluminum with different purities using the Dynamic Materials Model has shown that a domain corresponding to DRX occurs in power dissipation maps. On the basis of this analysis, the following conclusions were determined:

1. The DRX temperature is purity-dependent and is about 375 °C for 99.999 pct Al, 450 °C for 99.99 pct Al, 550 °C for 99.9 pct Al, and 600 °C for 99.5 pct Al.
2. The strain rate at which DRX occurs at these temperatures is 10^{-3} s^{-1}.
3. The maximum efficiency of power dissipation for the DRX process is about 55 pct, as compared to the ideal linear dissipator.
4. The characteristics of DRX in aluminum are similar to those of static recrystallization with regards to the sigmoidal grain size variation with temperature and the variation of recrystallization temperature with purity. However, the DRX temperature is significantly higher.

ACKNOWLEDGMENTS

The authors gratefully acknowledge the help received from Dr. P. Rodriguez, Dr. S.L. Mannan, and Mr. P. Venugopal of Indira Gandhi Center for Atomic Research, Kalpakkam, India, in providing the 5-9 purity aluminum and for their interest in this work. The support of the Department of Science and Technology, Government of India for the Processing Science Research is also acknowledged. One of the authors (YVRKP) is thankful to Dr. H.L. Gegel, formerly of Wright-Patterson Air Force Base, OH, and now with Universal Energy

Systems, Dayton, OH, for introducing him to this area of research and for many inspiring discussions.

REFERENCES

1. M.E. Kassner, M.M. Myshlyaev, and H.J. McQueen: *Mater. Sci. Eng.*, 1989, vol. 108A, pp. 45-61.
2. J.J. Jonas, C.M. Sellars, and W.J. McG. Tegart: *Met. Rev.*, 1969, vol. 14, pp. 1-24.
3. H.J. McQueen and J.J. Jonas: in *Plastic Deformation of Materials*, R.J. Arsenault, ed., Academic Press, New York, NY, 1975, p. 393.
4. H.J. McQueen, E. Evangelista, J. Bowles, and G. Crawford: *Met. Sci.*, 1984, vol. 18, pp. 395-402.
5. K.J. Gardner and R. Grimes: *Met. Sci.*, 1979, vol. 13, pp. 216-22.
6. M.A. Zaidi and T. Sheppard: *Met. Sci.*, 1983, vol. 17, pp. 219-28.
7. T. Sheppard, N.C. Parson, and M.A. Zaidi: *Met. Sci.*, 1983, vol. 17, pp. 481-90.
8. S.P. Belyayev, V.A. Likhachev, M.M. Myshlyayev, and O.N. Senkov: *Phys. Met. Metall.*, 1981, vol. 52, pp. 143-52.
9. Ch. Perdrix, M.Y. Perrin, and F. Montheillet: *Mem. Sci. Rev. Metal.* (in French), 1981, vol. 78, p. 309; Engl. Transl. Rep. UCIR-1623, Lawrence Livermore National Laboratory, Livermore, CA, 1986.
10. F. Montheillet: *Les Traitements Thermomecaniques* (in French), P. Costa, ed., Institut National des Sciences et Techniques Nucleaires, Saclay, France, 1981, p. 57; Engl. Transl. Rep. UCIR-1621, Lawrence Livermore National Laboratory, Livermore, CA, 1986.
11. L. Styczynski, W. Pachla, and S. Wojciechowski: *Met. Sci.* 1982, vol. 16, pp. 525-28.
12. H.J. McQueen, O. Knustad, N. Ryum, and J.K. Solberg: *Scripta Metall.*, 1985, vol. 19, pp. 73-78.
13. H.J. McQueen, J.K. Solberg, N. Ryum, and E. Nes: *Al Alloys—Physical and Mechanical Properties*, Engineering Materials Advisory Service, Warley, United Kingdom, 1986, p. 515.
14. J.J. Urcola and C.M. Sellars: *Acta Metall.*, 1987, vol. 35, pp. 2637-47.
15. J.J. Urcola and C.M. Sellars: *Acta Metall.*, 1987, vol. 35, pp. 2649-57.
16. T. Sheppard and D.S. Wright: *Met. Technol.*, 1979, pp. 215-23.
17. W. Roberts, H. Boden, and B. Ahlblom: *Met. Sci.*, 1979, vol. 13 (19), pp. 195-205.
18. R. Raj: *Metall. Trans. A*, 1981, vol. 12A, pp. 1089-97.
19. Y.V.R.K. Prasad, H.L. Gegel, S.M. Doraivelu, J.C. Malas, J.T. Morgan, K.A. Lark, and D.R. Barker: *Metall. Trans. A*, 1984, vol. 15A, pp. 1883-92.
20. H.L. Gegel, J.C. Malas, S.M. Doraivelu, and V.A. Shende: *Metals Handbook*, ASM, Metals Park, OH, 1988, vol. 14, pp. 417-38.
21. H. Ziegler: in *Progress in Solid Mechanics*, I.N. Sneddon and R. Hill, eds., North-Holland Publishing Company, Amsterdam, 1963, vol. IV, pp. 93-193.
22. I. Prigogine: *Science*, 1978, vol. 201, pp. 777-87.
23. J.C. Blade, J.W.H. Clare, and H.J. Lamb: *J. Inst. Met.*, 1959–60, vol. 88, pp. 365-68.
24. B. Bay: *Scripta Metall.*, 1970, vol. 4, pp. 489-94.
25. B. Bay and N. Hansen: *Metall. Trans. A*, 1984, vol. 15A, pp. 287-97.
26. S.S. Gorelik: *Recrystallization in Metals and Alloys*, Mir Publishers, Moscow, 1981, pp. 127-64.
27. W.M. Williams and R. Eborall: *J. Inst. Met.*, 1952–53, vol. 81, pp. 501-12.
28. M.E. Kassner, J.J. Oldani, and K.L. Cadwell: *The Variation of Torsional Ductility of High-Purity Aluminium with Temperature and Strain Rate*, Rep. UCRL-98000, Lawrence Livermore National Laboratory, Livermore, CA, 1988.
29. J.R. Cotner and W.J. McG. Tegart: *J. Inst. Met.*, 1969, vol. 97, pp. 73-78.